ACS APPLIED MATERIALS & INTERFACES

Research Article

www.acsami.org

Decoration of Spongelike $Ni(OH)_2$ Nanoparticles onto MWCNTs Using an Easily Manipulated Chemical Protocol for Supercapacitors

Deepak P. Dubal,*[,†] Girish S. Gund,[‡] Chandrakant D. Lokhande,[‡] and Rudolf Holze*[,†]

[†]Technische Universität Chemnitz, Institut für Chemie, AG Elektrochemie, D-09107 Chemnitz, Germany

[‡]Thin Film Physics Laboratory, Department of Physics, Shivaji University, Kolhapur, 416004 (M.S), India

Supporting Information

ABSTRACT: This study uses a "bottom-up" approach chemical method to coat nanocrystalline $Ni(OH)_2$ onto multiwalled carbon nanotubes (MWCNTs) for flexible supercapacitor electrodes, where the higher electronic conductivity of MWCNTs permits their use as the supporting backbone onto which $Ni(OH)_2$ can be deposited. The paper portrays the advantages of the facile successive ionic layer adsorption and reaction (SILAR) method for depositing $Ni(OH)_2$/MWCNT thin films onto large area flexible substrates. We demonstrate that these $Ni(OH)_2$/MWCNT films consist of a uniform coating of sponge-like $Ni(OH)_2$ on the MWCNT network structure using scanning electron micrographs and transmission electron micrographs; this structure is promising for supercapacitor applications. $Ni(OH)_2$/MWCNT films exhibit a specific capacitance of 1487 F g^{-1} at a scan rate of 5 mV s^{-1} in a 2 M KOH aqueous solution. The electrodes are generated using a simple three-beaker SILAR system at ambient conditions, thus providing an easy approach to fabricate high-power and high-energy flexible supercapacitors. $Ni(OH)_2$/MWCNTs demonstrate a good rate capability and excellent long-term cyclic stability (96% capacity retention after 1000 cycles). Such high-performance capacitive behavior indicates that $Ni(OH)_2$/MWCNT composites are promising electrode materials for the fabrication of supercapacitors. Thus, the method described in this paper provides a generalized route for the production of a wide range of $Ni(OH)_2$/MWCNT-based materials for applications beyond electrochemical energy storage. These encouraging results promote interest in developing such devices, including nontoxic and greener components, compared with current organic-based devices.

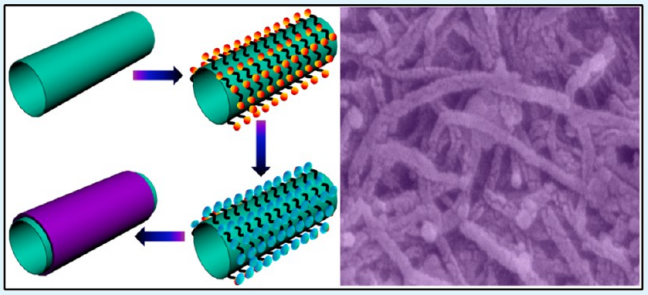

KEYWORDS: *SILAR, $Ni(OH)_2$/MWCNTs, thin films, spongy nanoparticles, electrochemical impedance, supercapacitor*

INTRODUCTION

Supercapacitor is nothing but the combination of advantages of both conventional capacitors, which have high power density and rechargeable batteries, which have high energy density. Recently, supercapacitors have attracted worldwide research interest because of the requirements of energy storage devices in many fields, such as in hybrid electric vehicles, mobile electronic devices.[1,2] Various materials have been investigated for applications as the electrodes in supercapacitors, including carboneous materials, conducting polymers, and transition-metal oxides.[3−5]

Multiwalled carbon nanotubes (MWCNTs), which are an excellent form of carbon, attract much attention as supercapacitor electrode material because of their unique mesoporous network, high electrochemically accessible surface area, outstanding electrical conductivity, and excellent chemical stability.[6] Furthermore, MWCNTs provide conducting pathway to facilitate a fast electrochemical kinetic process during high current density charge/discharge.[7,8] However, because of their limited surface area, the inherent capacitance of carbon nanotubes is small (~150 F g^{-1}).[6,9] Further increase in supercapacitance of MWCNTs is very hard to achieve since difficulties in controlling the pore size and electrochemically active surface area. To increase energy, as well as power density, transition metal oxides must be deposited within MWCNTs to form faradic pseudocapacitors. MWCNTs decorated with different materials, such as metal oxides (MnO_2, Co−Ni oxide, etc.) and conducting polymers (polyaniline, polypyrrole, etc.), have shown enhanced electrochemical performance.[10−12] Among the different transition metal oxides, amorphous hydrous RuO_2 is the most promising material for supercapacitors.[13] However, RuO_2 is expensive, toxic, and naturally less abundant, which limits its commercial use. Therefore, in recent years, great efforts have been taken to develop new and less expensive materials. Nickel hydroxide $Ni(OH)_2$, is one of the active transition metal hydroxide from the series of different metal oxides/hydroxides used for supercapacitors. Various properties, such as low cost, well-defined redox activity, layered structure, and high specific capacitance makes this material more attractive.[14,15] However, the poor electrical conductivity

Received: November 9, 2012
Accepted: March 7, 2013
Published: March 7, 2013

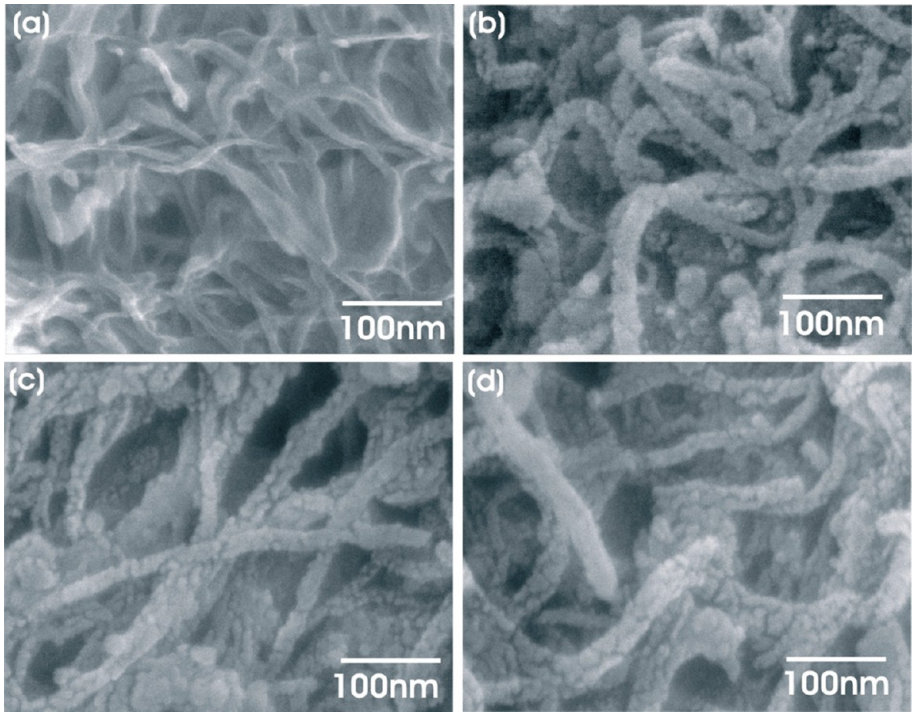

Figure 1. FESEM images of the morphological features of (a) pristine MWCNT and $Ni(OH)_2$/MWCNT thin films at (b) 30, (c) 57, and (d) 81 mg cm^{-2} mass loadings.

and low cycle life of pseudocapacitive $Ni(OH)_2$ restricted their practical applications.[16] To overcome these drawbacks, conducting additives, such as graphene, carbon nanotubes (CNTs), or carbonaceous species, must be introduced to form pseudocapacitive nanocomposites, having high values of supercapacitance with excellent cycling stability.

A recent approach is the decoration of $Ni(OH)_2$ nanoparticles directly onto the walls of MWCNTs. $Ni(OH)_2$/MWCNTs nanocomposite has 2D $Ni(OH)_2$ nanostructure, which maximize the active material utilization ratio and decrease the diffusion length significantly, this results in high specific capacitance and excellent rate capability. Further, MWCNTs framework confinement efficiently buffers the volume change of the pseudocapacitive materials during the long-term charging and discharging process, leading to high capacitance retention. In such a composite, $Ni(OH)_2$ with high surface area offers the desired high specific capacitance, and the MWCNT framework provides improved electrical conductivity, mechanical stability, and additional electrochemical double-layer capacitance. Growth of $Ni(OH)_2$ nanoparticles directly on CNTs is complicated. Fortunately, SILAR has emerged as one of the recent soft chemical solution methods useful for such synthesis, as the basic building blocks are ions instead of atoms. This process is advantageous because of layer by layer growth, for example, nanocomposite can built by alternating pseudocapacitive ($Ni(OH)_2$) layer and conducting CNTs layer, which is a promising pathway to enhance electrochemical properties. In addition, process results in excellent material utilization efficiency, provides good control of the film thickness and is specifically convenient for large area deposition. Since the deposition is carried out at or near room temperature oxidation and corrosion of metallic substrates can be avoided.[17]

Our efforts are focused on the development of a simple and inexpensive commercial synthesis route for the preparation of $Ni(OH)_2$/MWCNTs directly onto flexible substrates to achieve compatibility with supercapacitors. In addition, the SILAR grown films are characterized to study their structural, morphological, compositional, and surface area properties. The electrochemical properties of $Ni(OH)_2$/MWCNT films are also investigated using cyclic voltammetry, charge/discharge, and impedance techniques. The cyclic voltammetry measurements reveal that the $Ni(OH)_2$/MWCNT electrodes have a high specific capacitance, which can be attributed to the presence of the pseudocapacitive sponge-like $Ni(OH)_2$ nanoparticles connected to the electrically conductive MWCNTs. Finally, we demonstrate the unique advantages of the SILAR method, which include control of the thickness down to a nanometer scale and the availability of a large deposition area on flexible substrates (>30 cm^2).

RESULTS AND DISCUSSION

Material Preparation and Characterization. $Ni(OH)_2$/MWCNT thin films were produced by successive immersion of flexible stainless steel (FSS) substrates into separately placed cationic and anionic precursor solutions. According to the growth kinetics, the film grows by ion-by-ion deposition at nucleation sites on the immersed surface.[17] Briefly, functionalized MWCNTs were well dispersed into the deionized water using an ultrasonicator. When the FSS substrate was immersed in this solution, the MWCNTs were adsorbed onto the substrate because of the attractive force between the substrate and the MWCNTs in the solution. These forces may be cohesive forces, van der Waals forces, or other chemical attractive forces. In a second beaker, 0.1 M $NiSO_4$, which was used as a source of nickel, was added to an aqueous ammonia (NH_4OH) solution (25% extra pure) with constant stirring to make the solution alkaline. Initially, when the aqueous ammonia solution was added to the nickel sulfate, the ion product of $Ni(OH)_2$ exceeded the solubility product, and the

dx.doi.org/10.1021/am3026486 | ACS Appl. Mater. Interfaces 2013, 5, 2446−2454

solution became turbid because of the precipitation of $Ni(OH)_2$ according to:

$$NiSO_4 + 2NH_4OH \rightarrow Ni(OH)_2\downarrow + 2NH_4^+ + SO_4^- \quad (1)$$

However, further addition of surplus ammonia solution reduced the Ni^{2+} ion concentration by producing the complex ion of type $Ni(NH_3)_n^{2+}$ (n = 1–4), with n = 4 being the most stable co-ordination number.[18] Because of the complex formation, the solution becomes clear and transparent, which can be explained by the following reaction:

$$Ni(OH)_2 + 4NH_4^+ \rightarrow Ni(NH_3)_4^{2+} + 2H_2O + 2H^+ \quad (2)$$

When the substrate was immersed in the above solution, the $Ni(NH_3)_4^{2+}$ ions in the solution were preferentially adsorbed on the walls of the MWCNTs because of the electrostatic force of attraction between the $Ni(NH_3)_4^{2+}$ ions and the functionalized MWCNTs.

It is significant that deionized water with a few drops of H_2O_2 provides a source of OH^- ions upon heating at a temperature near the boiling point. H_2O_2 acts as catalyst, which provides an alternative path for the reaction by reducing the activation energy of chemical reaction. The reaction was followed by the immersion of the wet substrate into deionized water maintained at 343 K, where the chemical reaction between OH^- and the preadsorbed $Ni(NH_3)_4^{2+}$ ions at the surface of the MWCNTs results in the deposition of an adherent $Ni(OH)_2$ layer only a few nanometers in thickness according to:

$$Ni(NH_3)_4^{2+} + 2OH^- \rightarrow Ni(OH)_2 + 4NH_3\uparrow \quad (3)$$

The cycle of ion adsorption followed by oxidation reaction was repeated several times to achieve different film thicknesses. Finally, the $Ni(OH)_2$/MWCNT thin film was rinsed with deionized water several times to remove loosely bound and unreacted species. This step completed one SILAR cycle. The cycle was repeated several times to obtain films of different thicknesses. To increase the mechanical stability and electrical conductivity of the electrodes, $Ni(OH)_2$/MWCNTs were heat treated at 100 °C for 12 h under vacuum and then used for further characterizations.

Figure 1 presents FESEM images of the morphological features of the (a) pristine MWCNT and (b–d) $Ni(OH)_2$/MWCNT thin films at different mass loadings. MWCNTs are randomly spread all over the substrate with well-developed nanoscale pores. No aggregation and alignment of bundles of MWCNTs due to van der Waals interactions is observed. However, from Figure 1b–1d, the $Ni(OH)_2$/MWCNT films exhibit a rough surface in comparison with pristine MWCNTs. The outside surface of the MWCNTs is uniformly dotted with $Ni(OH)_2$ nanoparticles less than 10 nm in size, and the thickness of the $Ni(OH)_2$/MWCNTs films increases as the number of SILAR cycles increases (Supporting Information S4), which can be observed from the increase in the tube diameters. No aggregation of the $Ni(OH)_2$ nanoparticles off the MWCNT scaffold is observed in the composite, indicating that the nucleation occurs predominantly on the exterior surfaces of the MWCNTs. The growth mechanism for decorating $Ni(OH)_2$ nanoparticles on MWCNTs is depicted in Scheme 1. The oxygen-containing functional groups on the MWCNT act as anchoring or nucleation sites for the growth of $Ni(OH)_2$. Electrostatic forces of attraction between $Ni(NH_3)_4^{2+}$ ions in the solution and the polar oxygen functional groups introduced by the acid treatment causes the adsorption of $Ni(NH_3)_4^{2+}$ ions on these sites. Subsequently, OH^- reacts with the $Ni(NH_3)_4^{2+}$, which has been adsorbed on the surface of the MWCNT via electrovalent bonding to form the $Ni(OH)_2$ nanoparticles. Thus the selective heterogeneous nucleation and growth of spongelike $Ni(OH)_2$ nanoparticles is induced on the entire external surface of MWCNT. These nanoparticles provide high surface area and porous volume, which is feasible for high performance supercapacitor application.[19,20]

Scheme 1. Growth Mechanism for Decorating $Ni(OH)_2$ Nanoparticles on MWCNTs[a]

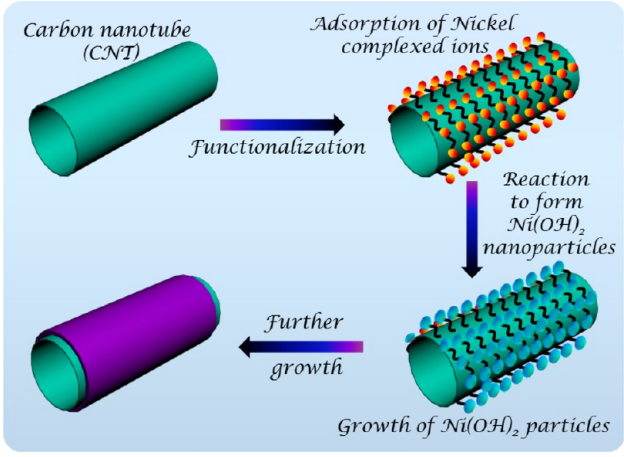

[a]The polar oxygen functional groups introduced by acid treatment act as nucleation sites. The $Ni(NH_3)_4^{2+}$ ions in the solution are adsorbed onto these sites. Subsequently, OH^- reacts with the $Ni(NH_3)_4^{2+}$ via electrovalent bonding to form $Ni(OH)_2$ nanoparticles. Finally, selective heterogeneous nucleation and growth of a sponge-like $Ni(OH)_2$ thin layer is induced on the MWCNTs.

TEM was used to characterize the nanostructure of the MWCNTs and $Ni(OH)_2$/MWCNT thin films (30 mg cm^{-2} mass loading), as shown in Figure 2. The TEM images of the MWCNTs in Figure 2A demonstrate a randomly oriented network structure of MWCNTs, where the MWCNTs are entangled together to form porous and loose morphologies. However, for the $Ni(OH)_2$/MWCNTs (Figure 2B–2C), spongelike $Ni(OH)_2$ nanoparticles were observed to be uniformly distributed throughout the MWCNT matrix. Such films exhibit good mechanical integrity and loose packing, leading to increase of the surface area of the MWCNTs. The corresponding SAED of the $Ni(OH)_2$/MWCNT electrode exhibited only disperse rings of graphite characteristic planes of (002), (100), and (110), which are indicative of the nanocrystalline nature of the deposited $Ni(OH)_2$. Because growth occurs through an ion by ion mechanism in the SILAR method, no aggregation of $Ni(OH)_2$ nanoparticles occurs on the walls of the MWCNTs. This result demonstrates that the $Ni(OH)_2$/MWCNT hybrid thin films can be easily and effectively synthesized using the SILAR method through selective heterogeneous nucleation onto MWCNTs. In addition, the MWCNTs provide a good original nanostructure for the nucleation, which strongly affects the nanostructure of the $Ni(OH)_2$.

XRD patterns of the MWCNT, $Ni(OH)_2$, and $Ni(OH)_2$/MWCNT powders are provided in Figure 2D. The characteristic graphitic (002) peak of the MWCNTs at 25.55° was clearly observed in both the MWCNT and $Ni(OH)_2$/MWCNT patterns.[21] The reflections along (100), (002), (100), (101), (102), (110), and (111) are consistent with β-phase nickel

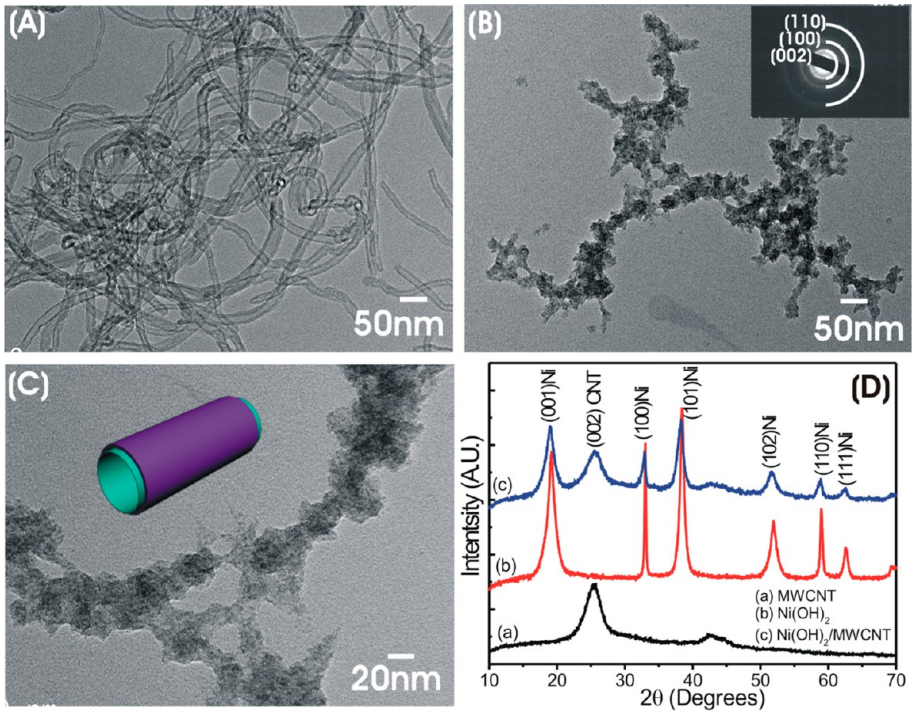

Figure 2. TEM images of (A) pristine MWCNT and (B–C) $Ni(OH)_2$/MWCNT (30 mg cm^{-2}) and (D) XRD patterns of MWCNTs, $Ni(OH)_2$, and $Ni(OH)_2$/MWCNTs powders.

hydroxide with a hexagonal brucite structure,[22] which matches well with the standard pattern (JCPDS 01-1047). Broad diffraction peaks indicate that the pure $Ni(OH)_2$ and $Ni(OH)_2$ coated onto the MWCNTs has a nanocrystalline nature. This phase is beneficial for supercapacitors because it creates penetration path through the bulk of the $Ni(OH)_2$ material, and the entire electrode material can be used for energy storage.

To further understand the composition of the final products, XPS was performed. Figure 3a presents the XPS general survey spectrum of the $Ni(OH)_2$/MWCNTs. The oxidation of CNTs and the decoration of $Ni(OH)_2$ on the walls of the CNTs are confirmed by the presence of the O1s and Ni2p peaks. The higher resolution XPS spectra for the Ni2p core level recorded in the range of 850–870 eV are shown in the inset of Figure 3a. The spectrum consisted of two spin–orbit doublets characteristic of Ni^{2+} and Ni^{3+} and two shakeup satellites. The binding energy of Ni $2p_{3/2}$ was about 855.8 eV, which is consistent with the previously reported value.[20] The nitrogen adsorption–desorption isotherm curve of the $Ni(OH)_2$/MWCNT sample and the corresponding pore size distribution (inset) are provided in Figure 3b. The nitrogen isotherm can be classified as a type IV isotherm with a small hysteresis loop. A small step of nitrogen adsorption and desorption branching occurs at a relative pressure (p/p_0) between 0.4 and 0.6, indicating the existence of mesopores. On the basis of the nitrogen adsorption–desorption isotherm, the BET surface area of the $Ni(OH)_2$/MWCNTs was calculated to be 153 m^2 g^{-1}. The pore size distribution data calculated from the adsorption branches of the nitrogen isotherms using the BJH (Barrett–Joyner–Halender) method suggests mesopores with a narrow pore size distribution, centered at 4.25 nm. These mesoporous networks of sponge-like nanoparticles provide low-resistance pathways through the porous structure, which helps to improve charge transport and power capability.[23] This result is

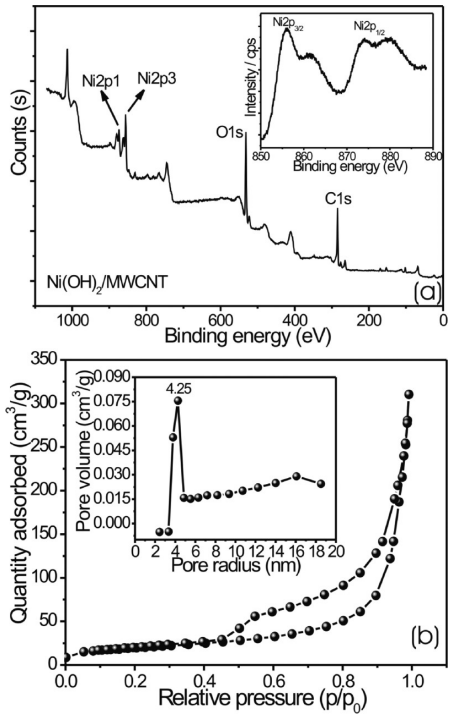

Figure 3. (a) XPS survey spectrum of $Ni(OH)_2$/MWCNT sample. Inset of XPS spectrum for Ni2p core level. (b) Nitrogen adsorption–desorption isotherms of $Ni(OH)_2$/MWCNT sample. Inset of panel b presents the pore size distribution curve of $Ni(OH)_2$/MWCNT.

significant for electrode materials because of the large specific capacitance and high-rate charge–discharge ability.

Electrochemical Analysis. Figure 4A presents the cyclic voltammetry curves of $Ni(OH)_2$, MWCNTs, and $Ni(OH)_2$/MWCNT in a 2 M KOH electrolyte at a 50 mV s^{-1} scan rate.

dx.doi.org/10.1021/am3026486 | ACS Appl. Mater. Interfaces 2013, 5, 2446–2454

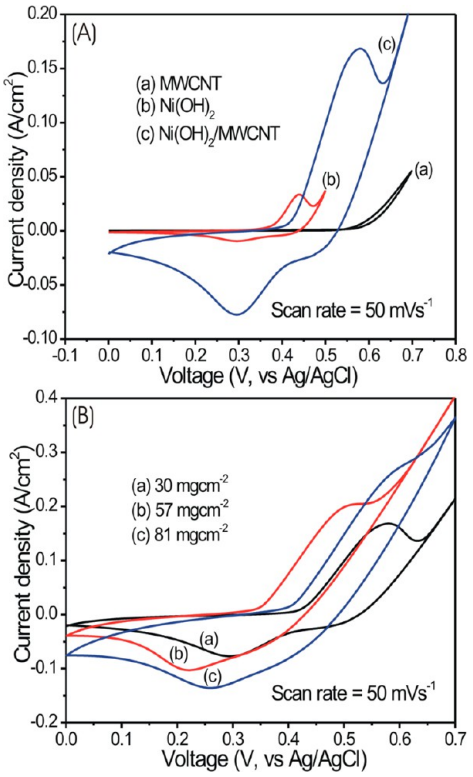

Figure 4. (A) Cyclic voltammetry (CV) curves of $Ni(OH)_2$, MWCNTs, and $Ni(OH)_2$/MWCNT and (B) mass-dependent CV of the $Ni(OH)_2$/MWCNT electrodes in 2 M KOH electrolyte at a 50 mV s^{-1} scan rate.

The shape of the CV indicates that the capacitance characteristic is different from the electric double layer capacitance, in which the shape is normally close to an ideal rectangular shape. From the curves, it is observed that (i) redox peaks are present for the $Ni(OH)_2$ and $Ni(OH)_2$/MWCNT curves, indicating that the capacity results mainly from a pseudocapacitive capacitance, which is based on a redox mechanism. This phenomenon may result from the β-$Ni(OH)_2$/β-NiOOH redox pair,[24] according to the following electrochemical reaction:

$$\beta\text{-Ni(OH)}_2 + \text{OH}^- \Leftrightarrow \beta\text{-NiOOH} + \text{H}_2\text{O} + \text{e}^- \quad (4)$$

The redox reaction of the nickel electrode is usually considered to be and intercalation and deintercalation of protons and electrons into and out of the bulk of the solid phase. (ii) The $Ni(OH)_2$/MWCNT composite provides a very high current compared with the $Ni(OH)_2$ and MWCNT samples. (iii) It is interesting to note that because of the MWCNTs, the potential window of the $Ni(OH)_2$ increases by 0.2 V.

We can fully utilize the advantages of the SILAR process, enabling precise capacity control of the electrodes by controlling the thickness of the $Ni(OH)_2$/MWCNT films. Figure 4B presents a mass-dependent CV of the $Ni(OH)_2$/MWCNT electrodes in the range from 30 to 81 mg cm^{-2} at a scan rate of 50 mV s^{-1}. Comparison of the curves reveals that the voltammetric current of the $Ni(OH)_2$/MWCNT electrode increases with film thickness, indicating that the specific capacitance decreases with increasing film thickness. A maximum value of 1156 F g^{-1} is obtained for a mass loading of 30 mg cm^{-2} at 50 mV s^{-1} scan rate. The value of specific capacitance decreases drastically from 1156 to 476 F g^{-1} with

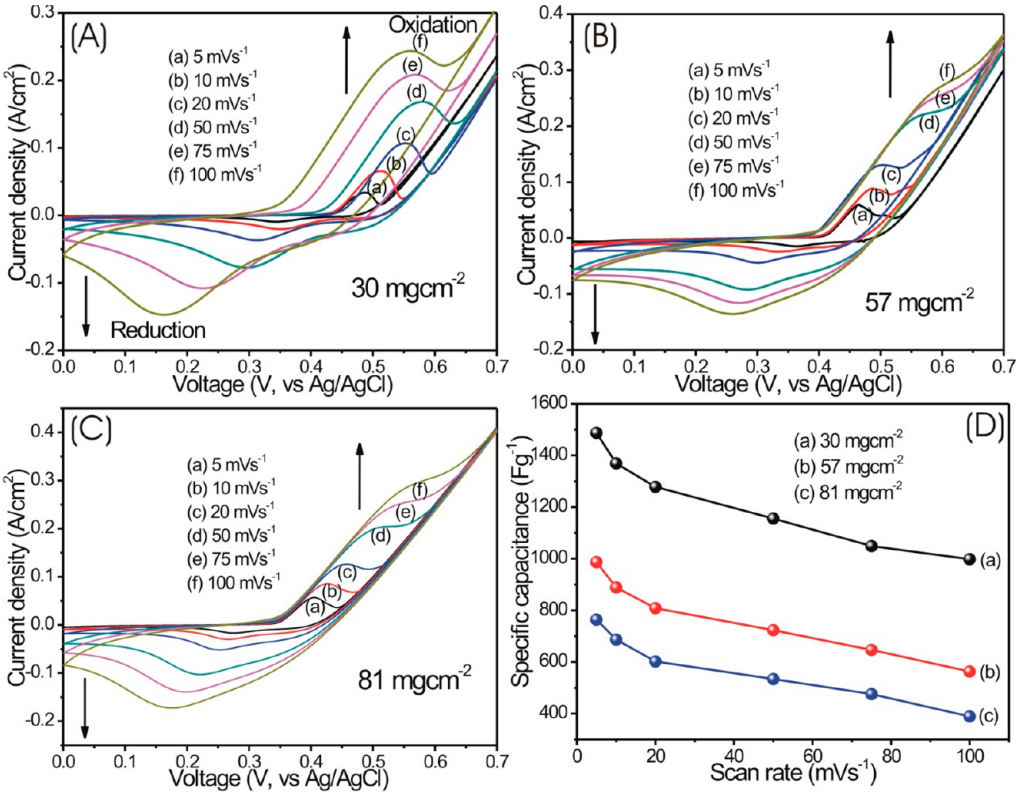

Figure 5. (A–C) CV curves of the $Ni(OH)_2$/MWCNT composites at different scan rates and (D) variations of the specific capacitance for $Ni(OH)_2$/MWCNT composites as a function of the scan rate for different mass loadings.

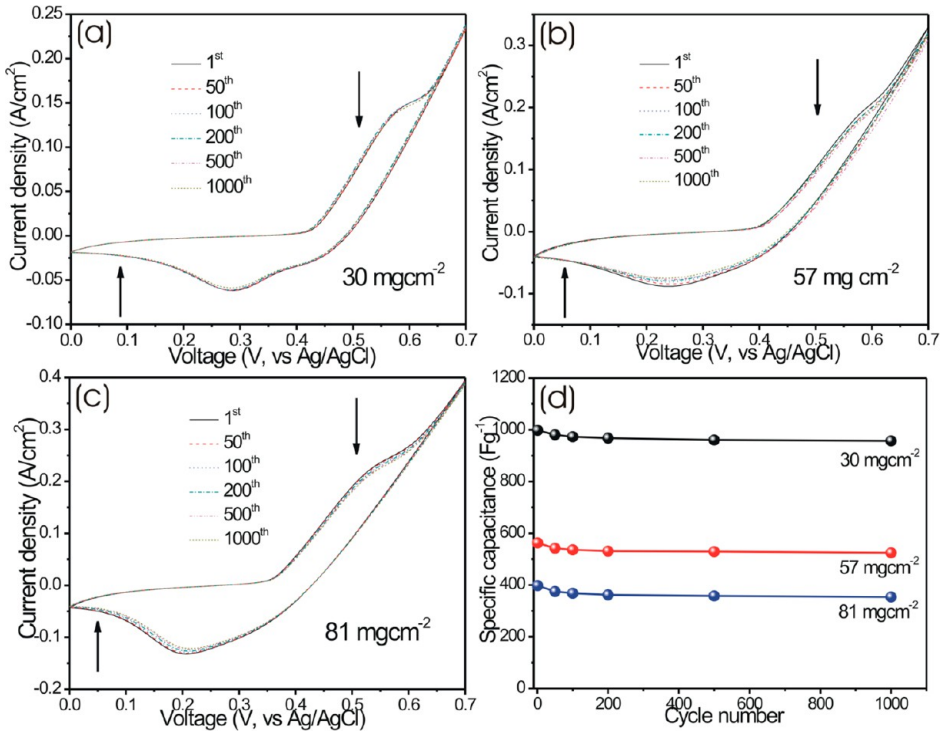

Figure 6. (a–c) CV curves of the $Ni(OH)_2$/MWCNT composites for different numbers of cycles at a 100 mV s^{-1} scan rate and (d) variations of the specific capacitance of $Ni(OH)_2$/MWCNTs with the number of cycles for different mass loading.

an increase in mass loading from 30 to 81 mg cm^{-2}. The specific capacitance values for the $Ni(OH)_2$/MWCNT electrodes of thicknesses smaller than 30 mg cm^{-2} could not be measured as these electrodes were observed to be unstable in the KOH electrolyte, and the results were not reproducible.

Figure 5A–C presents the cyclic voltammetry (CV) curves of the $Ni(OH)_2$/MWCNT composites at different scan rates for different thicknesses. The current under CV curves increases slowly with the scan rate which implies that the voltammetric current is directly proportional to the scan rates, indicating an ideally capacitive behavior.[25] The variation in the specific capacitance of the $Ni(OH)_2$/MWCNT composites as a function of the scan rate is plotted in Figure 5D. The nonideal rectangular shape of the CV curves is attributed to the fact, that at a high scan rate, the ions on the electrode are depleted rapidly with increasing current, while the ions in the electrolyte solution diffuse too slowly to satisfy the need for ions near the interface during the charging and discharging process.[26,27] The maximum values of specific capacitance achieved are 1487, 987, and 764 F g^{-1} at a 5 mV s^{-1} scan rate for 30, 57, and 81 mg cm^{-2} mass loadings, respectively (for the calculations, see Supporting Information S5). At a high scan rate of 100 mV s^{-1}, the specific capacitance still remains at 998 F g^{-1} for a 30 mg cm^{-2} mass loading. In addition, the thin $Ni(OH)_2$ layer provides a short diffusion path for ion transport and a high surface area. Moreover, the core MWCNTs, with a higher electrical conductivity than that of $Ni(OH)_2$, serves as a fast path for the transport of electrons. Because of the synergetic contribution from $Ni(OH)_2$ and the MWCNTs, the high-surface area and porous network structure allow a higher rate of solution infiltration and facilitate ion insertion/extraction and electron transport in the electrode.[28−30]

Lin et al.[21] prepared a NiO/CNT composite hydrothermally and reported a specific capacitance of 1329 F g^{-1}, as well as a good cycle life over 100 cycles. Nam et al.[31] reported NiO/CNT films prepared using electrochemical precipitation, and a high specific capacity of 1000 F g^{-1} was obtained; however, the prepared method used was very complex. Nam and Kim et al.[24] reported a specific capacitance of 671 F g^{-1} for electrochemically deposited $Ni(OH)_2$/MWCNT films. The values reported in the present investigation are higher than those reported earlier for $Ni(OH)_2$/MWCNT electrodes. This result is believed to be due to (i) the low temperature method of preparation, (ii) the sponge-like nature of the $Ni(OH)_2$ material and (iii), the fact, that in all of the above reports the $Ni(OH)_2$ nanoparticles are only mixed with MWCNTs that are not uniformly attached to the walls.

The cycling life test for the $Ni(OH)_2$/MWCNT electrode for different mass loading was performed at a scan rate of 100 mV s^{-1} over 1000 cycles as shown in Figure 6. It is seen that all the CV curves are overlapping each other which indicates good cycling stability. The specific capacitance decreases slightly after 1000 cycles. It is interesting that the decrease of specific capacitance is 4%, 7%, and 11% of the maximum specific capacitance for 30, 57, and 81 mg cm^{-2}, respectively. These results demonstrate that an active electrode material, that is, $Ni(OH)_2$, is very stable during the cycling test. The CV cycling test of the $Ni(OH)_2$/MWCNT film suggests that the synergetic interaction between the MWCNTs and $Ni(OH)_2$ significantly improved the electrical properties and the mechanical stability of the electrode.

A good electrochemical energy storage device can provide a high energy density at a high charge/discharge rate. The constant current charge/discharge curves of the $Ni(OH)_2$/MWCNT thin films at different densities for 30 mg cm^{-2} are shown in Figure 7A. The charging curves are very symmetric with their corresponding discharge counterparts. Notably, the voltage loss is low, indicating that the internal resistance is low.

dx.doi.org/10.1021/am3026486 | ACS Appl. Mater. Interfaces 2013, 5, 2446−2454

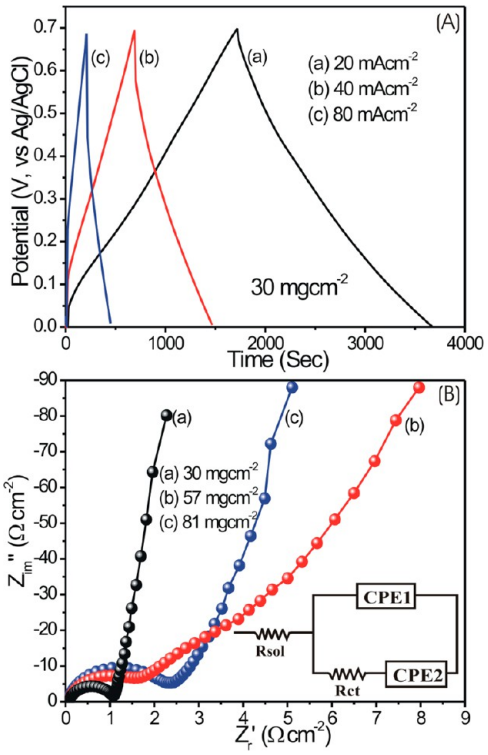

Figure 7. (A) Constant current charge/discharge curves of the $Ni(OH)_2$/MWCNT thin films at different densities for 30 mg cm^{-2} mass loading and (B) Impedance spectra from 10^3 to 10^{-3} Hz of $Ni(OH)_2$/MWCNT thin films for different mass loadings with inset representing equivalent circuit for $Ni(OH)_2$/MWCNT. Rsol, solution resistance; Rct, charge transfer resistance; CPE1 and CPE2, constant-phase elements.

The specific capacitance is calculated from the charge/discharge curves using the following relationship:[32]

$$Cs = \frac{I \times \Delta t}{\Delta V \times m} \quad (5)$$

where Cs is the specific capacitance, I is the charge/discharge current, Δt is the discharge time, ΔV is 0.7 V, and m is the mass of active material within the electrode. The $Ni(OH)_2$/MWCNT electrode clearly had good electrochemical reversibility and a large specific capacitance of 1537 F g^{-1}. The value of specific capacitance obtained by the charge/discharge and CV technique are comparable.

The impedance plots in Figure 7B reveal a partial semicircle for the high-frequency component because of the Faradaic charge transfer resistance and a nearly straight line along the imaginary axis at low frequencies because of the mass transport limit. The high-frequency intercept of the semicircle on the real axis yields the solution resistance (Rsol), and the diameter provides the charge-transfer resistance (Rct) over the interface between the $Ni(OH)_2$/MWCNT electrode and electrolyte.[33] The slope of the straight line in the low frequency range because of the Warburg resistance is a result of the frequency dependence of ion diffusion from the electrolyte solution to the electrode interface. The equivalent circuit in accordance with the above Nyquist plot is presented in the inset of Figure 7b. The existence of CPE may be due to (i) inhomogeneity at the electrode−electrolyte interface causing the distribution of relaxation times, (ii) porosity, (iii) the nature of the electrode, and (iv) the active disorder associated with diffusion. Here, in $Ni(OH)_2$/MWCNTs, the redox process occurs due to the diffusion of K^+ ions through the $Ni(OH)_2$/MWCNT material. The incorporation of two CPE elements in the equivalent circuit corresponds to the porosity of the electrode and the semi-infinite diffusion of the cations. A similar equivalent circuit has also been proposed for manganese oxide film electrodes.[34] The charge-transfer resistance at the solid−liquid interface increases in the following order: 30 < 57 < 81 mg cm^{-2}. If the charge-transfer resistance is smaller, the pseudocapacitor provides higher specific capacitance values.[35] From the Nyquist curves, the slope of the $Ni(OH)_2$/MWCNT electrode is steeper, implying that the thin sponge-like structures of $Ni(OH)_2$ can significantly enhance the diffusion of solvated cations to the porous electrodes. Figure 8 provides a schematic representation of the layer-by-layer assembly of the $Ni(OH)_2$/MWCNT thin films. Furthermore, digital photographs indicate

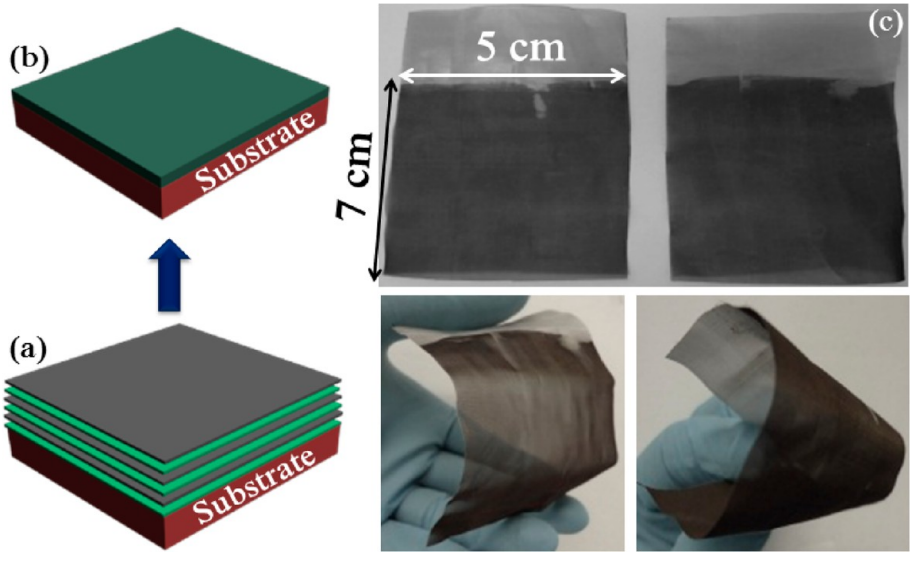

Figure 8. (a, b) Schematic representation of layer-by-layer assembly of $Ni(OH)_2$/MWCNT thin films. (c) Digital photographs of large-area $Ni(OH)_2$/MWCNT thin films on flexible stainless steel substrates.

the large area $Ni(OH)_2$/MWCNT thin films on flexible stainless steel substrates. These encouraging results stimulate interest in developing such flexible devices, including nontoxic and greener components compared with the current organic-based devices.

CONCLUSIONS

In summary, we developed a bottom-up approach lucrative chemical method to decorate nanocrystalline $Ni(OH)_2$ on MWCNTs. The porous MWCNT network generated via alternating layer-by-layer assembly creates fast electronic and ion conducting channels in the presence of an electrolyte, and the conformal coating of $Ni(OH)_2$ on MWCNTs provides high capacitance, which indicates that these systems can provide a platform to design high-performance electrodes for supercapacitor applications. The high capacitance and excellent rate capability of $Ni(OH)_2$/MWCNT electrodes can be attributed to the electrode nanostructure, where sponge-like $Ni(OH)_2$ nanoparticles are supported on a high-packing density, porous MWCNT network with adequate access to electrons and ions in the electrolyte. The ability to generate high electrode capacitances and the precise control of thickness and capacity from simple SILAR processes at ambient conditions suggests a promising approach for the creation of electrodes in a controlled manner. We believe that these high-capacitance $Ni(OH)_2$/MWCNT flexible electrodes and the general approach for the fabrication of nanostructured electrodes can be applied to design novel electrode materials for supercapacitor, battery and sensor applications.

EXPERIMENTAL SECTION

The synthesis process of $Ni(OH)_2$/MWCNT thin film via the simple SILAR method is based on a sequential reaction on the substrate surface by successive immersion of the substrate into separately placed cationic and anionic precursor solutions at room temperature. A three-beaker SILAR system is used for deposition of the $Ni(OH)_2$/MWCNT thin film directly onto stainless steel (SS) substrates. Briefly, 0.01 g of functionalized MWCNTs is sonicated in 50 mL Milli-Q water (18 MΩ·cm) for several hours to form stable dispersions. These dispersed MWCNTs are collected in the first beaker. For a brief description of the functionalization of MWCNTs, see Supporting Information S1. A second beaker contains aqueous nickel sulfate (0.1 M) solution, which acts as a source of Ni^{2+} ions that is made alkaline by the addition of aqueous ammonia solution to make the pH of the solution ~12. Finally, the third beaker contains deionized water with a few drops of H_2O_2 (6%) solution, which is maintained at 343 K and acts as source of hydroxyl ions. First, the ultrasonically treated and well-cleaned SS substrates are dipped in the MWCNT solution for 20 s, in which the MWCNTs are adsorbed onto the substrate surface. Next, the substrate was dipped in an alkaline nickel sulfate solution for 10 s for the nickel complex ions to adsorb onto the surface of the preadsorbed MWCNTs. After immersion of the substrate into the H_2O_2 solution maintained at 343 K for 10 s, a reaction occurred at the MWCNT surfaces to form $Ni(OH)_2$ nanoparticles. This cycle was repeated several times to increase the thickness of the $Ni(OH)_2$/MWCNT thin film. The schematic of SILAR method for deposition of $Ni(OH)_2$/MWCNTs is illustrated in Supporting Information S2. To fabricate $Ni(OH)_2$/MWCNT thin films of different thicknesses, the number of SILAR cycles was varied and digital images are shown in Supporting Information S3.

The surface morphology was studied using scanning electron microscopy (JEOL JSM-7500F). Transmission electron micrographs (TEM) and selected area electron diffraction (SAED) observations were conducted using JEOL JEM-2100 operated at 200 kV. A crystallographic study was performed using a Rigaku Rotalflex RU-200B diffractometer using a Cu Kα (λ = 1.5418 Å) source with a Ni filter at 40 kV and 40 mA at a scan rate of 0.02 s^{-1}. X-ray photoelectron spectroscopy (XPS, also known as Electron Spectroscopy for Chemical Analyzer or ESCA) was performed with a VG Multilab 2000 from Thermo VG Scientific U.K. N_2 adsorption/desorption was determined by Brunauer–Emmett–Teller (BET) measurements using an ASAP-2010 surface area analyzer. Cyclic voltammograms (CVs) were performed with a AMETEK Solartron analytical system model 1400 with an electrochemical cell consisting of $Ni(OH)_2$ as the working electrode and Ag/AgCl and platinum as the reference and counter electrodes, respectively. 8-Channel advanced battery cycler (WonATech-WBCS-3000 model) is used to carry out galvanostatic charge/discharge measurement. Electrochemical impedance spectroscopy (EIS) measurements were recorded using the multi-impedance test system in the frequency range of 10 kHz to 10 mHz with an AC amplitude of 10 mV.

ASSOCIATED CONTENT

Supporting Information

Description of the functionalization of MWCNTs, schematic illustration of the SILAR method for the deposition of $Ni(OH)_2$/MWCNT thin films, photographs of $Ni(OH)_2$/MWCNT thin films on an FSS substrate, SEM, TEM, SAED, and HRTEM images of $Ni(OH)_2$ thin films, EDX patterns for $Ni(OH)_2$/MWCNT thin films. This information is available free of charge via the Internet at http://pubs.acs.org/

AUTHOR INFORMATION

Corresponding Author

*Tel.: +49-371-531-982874. Fax: +49- 371-531-21269. E-mail: dubaldeepak2@gmail.com (D.P.D.); rudolf.holze@chemie.tu-chemnitz.de (R.H.).

Notes

The authors declare no competing financial interest.

ACKNOWLEDGMENTS

One of the authors (D.P.D.) appreciates the award of a Humboldt Fellowship of the Alexander von Humboldt Foundation (AvH), Germany. Authors are also thankful to Mr. Torsten Jagemann from Institute of Physics, Chemnitz University of Technology for SEM measurements.

REFERENCES

(1) Miller, J. R.; Simon, P. *Science* **2008**, *321*, 651–652.
(2) Simon, P.; Gogotsi, Y. *Nat. Mater.* **2008**, *7*, 845–854.
(3) Bak, S. M.; Kim, K. H.; Lee, C. W.; Kim, K. B. *J. Mater. Chem.* **2011**, *21*, 1984–1990.
(4) Lee, S. W.; Kim, J.; Chen, S.; Hammond, P. T.; Horn, Y. S. *ACS Nano* **2010**, *4*, 3889–3896.
(5) Hou, Y.; Cheng, Y.; Hobson, T.; Liu, J. *Nano Lett.* **2010**, *10*, 2727–2733.
(6) Joo, S. H.; Choi, S. J.; Oh, I.; Kwak, J.; Liu, Z.; Terasaki, O.; Ryoo, R. *Nature* **2001**, *412*, 169–172.
(7) Tang, W.; Hou, Y. Y.; Wang, X. J.; Bai, Y.; Zhu, Y. S.; Sun, H.; Yue, Y. B.; Wu, Y.; Zhu, K.; Holze, R. *J. Power Sources* **2012**, *197*, 330–333.
(8) Tang, W.; Gao, X.; Zhu, Y.; Yue, Y.; Shi, Y.; Wu, Y.; Zhu, K. *J. Mater. Chem.* **2012**, *22*, 20143–20145.
(9) Lee, S. W.; Kim, B. S.; Chen, S.; Horn, Y. S.; Hammond, P. T. *J. Am. Chem. Soc.* **2009**, *131*, 671–679.
(10) Wang, B.; Cheng, J.; Wu, Y.; Wang, D.; He, D. *J. Mater. Chem. A* **2013**, *1*, 1368–1373.
(11) Salunkhe, R. R.; Jang, K.; Lee, S.; Yu, S.; Ahn, H. *J. Mater. Chem.* **2012**, *22*, 21630–21635.
(12) Fan, H.; Wang, H.; Zhao, N.; Zhang, X.; Xu, J. *J. Mater. Chem.* **2012**, *22*, 2774–2780.

(13) Lokhande, C. D.; Dubal, D. P.; Joo, O. S. *Curr. Appl. Phys.* **2011**, *11*, 255−270.
(14) Jiang, H.; Zhao, T.; Li, C.; Ma, J. *J. Mater. Chem.* **2011**, *21*, 3818−3823.
(15) Zhang, J.; Kong, L. B.; Cai, J. J.; Li, H.; Luo, C.; Kang, L. *Microporous Mesoporous Mater.* **2010**, *132*, 154−162.
(16) Patil, U. M.; Gurav, K. V.; Fulari, V. J.; Lokhande, C. D.; Joo, O. S. *J. Power Sources* **2009**, *188*, 338−342.
(17) Hodes, G. *Chemical Solution Deposition of Semiconductor Films*; Marcel Dekker, Inc.: New York, 2002; p 40.
(18) *Comprehensive Coordination Chemistry*, Vol. 5; Wilkinson, G. Ed.; Pergamon Press: Oxford, U.K., 1987; p 71.
(19) Hu, G.; Li, C.; Gong, H. *J. Power Sources* **2010**, *195*, 6977−6981.
(20) Chen, W.; Yang, Y.; Shao, H. *J. Power Sources* **2011**, *196*, 488−494.
(21) Lin, P.; She, Q.; Hong, B.; Liu, X.; Shi, Y.; Shi, Z.; Zheng, M.; Dong, Q. *J. Electrochem. Soc.* **2010**, *157*, A818−A823.
(22) Zhou, G. T.; Yao, Q. Z.; Wang, X.; Yu, J. C. *Mater. Chem. Phys.* **2006**, *98*, 267−272.
(23) Dubal, D. P.; Lee, S. H.; Kim, J. G.; Kim, W. B.; Lokhande, C. D. *J. Mater. Chem.* **2012**, *22*, 3044−3052.
(24) Nam, K. W.; Kim, K. H.; Lee, E. S.; Yoon, W. S.; Yang, X. Q.; Kim, K. B. *J. Power Sources* **2008**, *182*, 642−652.
(25) Dubal, D. P.; Fulari, V. J.; Lokhande, C. D. *Microporous Mesoporous Mater.* **2012**, *151*, 511−516.
(26) Rakhi, R. B.; Cha, D.; Chen, W.; Alshareef, H. N. *J. Phys. Chem. C* **2011**, *115*, 14392−14399.
(27) Liu, R.; Duay, J.; Lee, S. B. *Chem. Commun.* **2011**, *47*, 1384−1404.
(28) Fan, H.; Wang, H.; Zhao, N.; Zhang, X.; Xu, J. *J. Mater. Chem.* **2012**, *22*, 2774−2780.
(29) Ghimbeu, C. M.; Pinero, E. R.; Fioux, P.; Beguin, F.; Guterl, C. V. *J. Mater. Chem.* **2011**, *21*, 13268−13275.
(30) Mao, L.; Zhang, K.; Chan, H. S. O.; Wu, J. *J. Mater. Chem.* **2012**, *22*, 1845−1851.
(31) Nam, K. W.; Lee, E. S.; Kim, J. H.; Lee, Y. H.; Kim, K. B. *J. Electrochem. Soc.* **2005**, *152*, A2123−A2129.
(32) Liu, C. G.; Lee, Y. S.; Kim, Y. J.; Song, I. C.; Kim, J. H. *Synth. Met.* **2009**, *159*, 2009−2012.
(33) Dubal, D. P.; Dhawale, D. S.; Salunkhe, R. R.; Lokhande, C. D. *J. Alloys Compd.* **2012**, *496*, 370−375.
(34) Dubal, D. P.; Dhawale, D. S.; Salunkhe, R. R.; Lokhande, C. D. *J. Electrochem. Soc.* **2010**, *157*, A812−A817.
(35) Girija, T. C.; Sangaranarayanan, M. V. *J. Power Sources* **2006**, *159*, 1519−1526.